IJCBR

INTERNATIONAL JOURNAL OF CANCER AND BIOMEDICAL RESEARCH

Adipose mesenchymal stem cell-based therapy: Anticancer molecular mechanisms in hepatoma model and bone marrow

Mona M. Atia, Ebtehal T. Sallam, Hanem S. Aly and Alshaimaa A. Alghriany

EKB Egyptian Knowledge Bank
بنك المعرفة المصري

■■■ RESEARCH ARTICLE

Adipose mesenchymal stem cell-based therapy: Anticancer molecular mechanisms in hepatoma model and bone marrow

Mona M. Atia[1], Ebtehal T. Sallam[1,2], Hanem S. Aly[1] and Alshaimaa A. Alghriany[1]

[1]Department of Zoology, Faculty of Science, Assiut University, Assiut, Egypt
[2]Department of Biology, Faculty of Education, Taiz University, Yemen

■■■ ABSTRACT

Background: Adipose-derived mesenchymal stem cells (AD-MSCs) can be used as therapeutic agents for the treatment of patients with HCC **Aim:** The study aimed to establish an animal model for hepatocellular carcinoma (HCC) by using diethyl nitrosamine (DEN) and carbon tetrachloride (CCl_4) in a short time. **Materials and Methods:** Forty-five female rats were subdivided into three groups: control (G1), HCC model (G2), and therapeutic (G3). Each rat in the G2 groups was injected with DEN and after 1 week was injected again with CCl_4, whereas G3 rats were injected with AD-MSCs immediately after the tumor appeared. **Results:** The injection of DEN/CCl_4 was correlated with the increase in alanine transaminase, aspartate aminotransferase, and alpha-fetoprotein levels. Also, it caused oxidative stress as indicated by an increase in nuclear factor-erythroid factor 2-related factor-2 (Nrf2), vascular endothelial growth factor levels, and fibrosis. However, BCL2-associated X protein (BAX) was decreased. Transplantation of AD-MSCs induced apoptosis by increasing BAX and decreasing Nrf2 levels, which significantly inhibited angiogenesis. Histologically, our results indicated that AD-MSCs alleviated hepatocellular carcinoma, fibrosis, and nuclear morphology. Additionally, the bone marrow (BM) maturation index ratio parameter was restored to a normal stage. **Conclusion:** AD-MSCs have a wide range of targeted anticarcinogenic properties and can regenerate BM precursors of cellularity.

Keywords: Anticancer; AD-MSCs; BM maturation index ratio; HCC model

■■■ ARTICLE INFO

Graphical abstract shows the anticancer mechanisms of AD-MSCs in hepatoma model, Total bone marrow cells (TBMC) and BM maturation index ratio (MIR).

INTRODUCTION

Hepatocellular carcinoma (HCC) is an end-stage liver disease that develops as a complication of fibrosis, cirrhosis, and malignancy (Memon et al., 2020). Worldwide, it ranks as the fifth major type of primary liver cancer and the second major cause of related mortality (Ding et al., 2021). In rats, diethyl nitrosamine (DEN) is the most commonly used chemical to stimulate the progression of cancer, which reduces levels of apoptosis (Memon et al., 2020). DEN followed by recurrent CCl_4 administration initiated a cancer model (Uehara et al., 2021). Several nuclear abnormalities in the rat liver and hepatocellular damage induced by reactive oxygen species (ROS) and DEN led to HCC (Mohamed et al., 2019). As a biomarker, alanine transaminase (ALT), aspartate aminotransferase (AST), and alpha-fetoprotein (AFP) are helpful only for the diagnosis of early HCC without other clinical information (Ding et al., 2020).

An inflammatory microenvironment generated by prolonged inflammatory cells and factors may also transform into an immunosuppressive microenvironment, thereby promoting angiogenesis and tumor progression. Immunotherapy is a novel and efficient tumor therapy (Cheng et al., 2020). Also, developing new therapeutics that target cell cycle and apoptosis dysregulation, inflammation, and fibrogenesis is crucial (Galicia-Moreno et al., 2021). The bone marrow (BM) is one of the body's largest lymphoid organs, the dominant site of hematopoiesis, and the most targeted organ for chemical injury (Ismael et al., 2019). Therefore, BM indicates the presence of cellularity changes in the BM and hematologic malignancy (Schwartz et al., 2019). In BM smears, cytological analysis can be used to determine affected cell lines (Pernecker et al., 2017), the presence of cellularity changes, and hematologic malignancy (Schwartz et al., 2019).

Mesenchymal *stem cells* (*MSCs*) are also *known* as medicinal signaling cells because they are multipotent progenitor cells that develop naturally in the body and stimulate hematopoiesis (Fathi et al., 2019; Qu et al., 2020). Functionally, they have the capability of self-renewal, proliferation, and regenerating tissues (Wang et al., 2021). Furthermore, it is the first choice for clinical applications in cancer therapies (Javan et al., 2019). Adipose, BM, and umbilical cord stem cells are the most common sources of stem cells (Wang et al., 2021). Inhibiting the proliferation of tumor cells is one way in which MSCs can affect hematologic malignancies (Fathi et al., 2019). MSCs release anti-inflammatory mediators such as interleukin-10 (IL-10) or transforming growth factor (TGF) β, which blocks the vascular endothelial growth factor (VEGF) angiogenesis pathway.

Subsequently, it induces apoptosis by secreting cytotoxic agents such as tumor necrosis factor-related apoptosis-inducing ligands and preventing the activation of Polycomblike2 (PCL2) in cancerous cells (Wang et al., 2021). The study aims to focus on establishing an HCC animal model by using DEN and CCl4 in a short time. Additionally, novel molecular pathways for AD-MSC-based therapy on HCC models were evaluated by modulating VEGF, Nrf2, and BAX signaling. Also, changes in BM maturation index ratios and AD-MSCs' role in regenerating BM precursors were determined.

MATERIAL AND METHODS
Drug & Animals

DEN and CCl_4 were supplied from the USA: (CCl_4; Sigma, CAS 56-23-5), (DEN; Sigma, CAS 55-18-5). Adult rats (12-week-old) were injected with a single dose of DEN (100 mg/kg, B.W. of I.P.) diluted in 15 mL of PBS (0.67%, w/v final). After 1 week of administration, doses of CCl_4 (0.2 mL/kg B.W. of I.P.) were diluted in corn oil to a final amount of 10 mL (0.01%, v/v) and injected twice a week for two weeks (Caviglia & Schwabe, 2014). Adult female rats (n = 45) with a total weight of 150–200 g was considered. One week prior to the experiment, the animals were allowed to be acclimatized to standard laboratory conditions.

Ethical approval

Under the National Institutes of Health criteria for the use of experimental animals; The research protocol used in the present study was reviewed and accepted by the medical ethics committee of Assiut University's Faculty of Medicine; Egypt, (IRB no: 17300705).

Experimental design

In this study, animals were randomized and subdivided into three groups: G1, G2, and G3. G1 (n = 15): was served as a control group without any treatments, G2 (n = 15): was considered as the HCC model group, and G3 (n = 15): was designated as a therapeutic group, each rat of the G3 group was injected with AD-SCs/0.5 mL PBS (0.65×10^6) immediately after a tumor appeared (8 weeks), then consumed into the caudal vein, and sacrificed, after 14 days of AD-MSC transplantation. The total experiment lasted 74 days.

Methods
Isolation of AD-MSCs

The protocol for isolating AD-MSCs was identical to the previous procedure (Atia & Alghriany, 2021). In brief, adult male rats' adipose tissues were sliced into pieces and rinsed with sterile PBS (Lonza, Swiss). The pieces were subsequently enzymatically digested for 45 min using collagenase type II (Sigma-Aldrich, St. Louis, MO, USA) (0.25% in PBS and 20% FBS). The falcon tubes (50 mL) were rotated every 10 min during the digestion incubation at 37°C, after which the collagenase activity was stopped by the addition of FBS. After centrifugation, the cell pellet containing the AD-MSCs was reconstituted in 12 mL of culture media (DMEM, Dulbecoos Modified Eagle Medium). The suspension was filtered using a cell strainer (40 μm) before being plated on 10 cm culture dishes. For two weeks, the cells were cultured at 37 degrees Celsius and 5% CO_2 until confluence reached approximately 80%, and AD-MSCs were transplanted at P3.

AD-MSC characterization via immunocytochemistry

For 20 min at room temperature, cells were fixed with 4% paraformaldehyde. PBS was used to wash the cells three times for 5 min each. The cells were permeabilized for 5 min in PBS with fresh 0.2% Triton X-100 (Marchenko & Flanagan, 2007). Secondary antipolyvaletstain was also used according to the manufacturer's instructions. The slides were then incubated with primary antibodies against CD105, CD90 (2:100), and CD45 (1:100) (Thermo Fisher, USA) for 1 h at room temperature. The Ultra-Tek

polyvalent goat anti-mouse horseradish peroxidase (HRP) was purchased from Sky Tek Laboratories, Logan, Utah, 84323, USA. The stain was added and incubated at room temperature for 10 min. The cells were immersed in the 3,3'-diaminobenzidine (DAB) substrate mix solution for 5 min (Atia & Alghriany, 2021).

Histopathological examination of liver carcinoma

Tiny liver sections were freshly taken and rapidly fixed in 10% neutral buffered formalin (pH 7.2) for histology and histopathological examination; liver sections were routinely processed using the paraffin-embedded technique. Subsequently, they are washed and dehydrated in an ascending grade of ethanol solutions (70-100%) to remove water, cleared in xylene, and then embedded in wax. A rotatory microtome was utilized to slice paraffin blocks into 5 μm thickness and be deparaffinized (dewaxed) in xylene, and finally, the standard staining procedure of Masson Tri Chrome stain was followed for type I collagen fiber (Suvarna et al., 2018). Examination and photography were carried out by using a digital camera (Toup Tek ToupView, Copyright© 2019, Version:x86, Compatible: Windows XP/Vista/7/8/10, China) and a computer connected to a light microscope (Olympus CX31, Japan).

Histopathological and Fibrosis Scores

Histopathological lesions stained with H&E and MTC were magnified and randomly imaged at x40 for scores 1&2. **Score 1:** for neoplastic lesions, five parameters were performed, Fatty change (Steatosis), inflammatory cell infiltration, Degeneration, Eosinophilic inclusion, and Granulomas (Heijnen et al., 2003). **Score 2:** for the fibrosis index, a random positive portion of the collagen fiber was measured as prior reported by Arjmand et al. (2020).

Biochemical Investigation assay

Serum ALT and AST parameters were determined using the appropriate kits (Boehringer Mannheim, Mannheim, Germany) following the manufacturer's recommendations. AFP levels in rat blood serum were measured at 450 nm using an

enzyme-linked immunosorbent assay (ELISA) test kit (Spectrum Diagnostics Company, Egypt).

Immunohistochemistry study

Formalin-fixed liver tissues in 10% neutral buffered with pH 7.2, paraffin-embedded tissues were sectioned, then cleared, and rehydrated in a grade of ethanol solutions (100%–70%) and submerged in water. Antigens were extracted by boiling the slides in 1 mM ethylenediaminetetraacetic acid (EDTA) for 10 min, emerging sections in 3% H_2O_2 for 10 min. Each section was put in a blocking solution at room temperature for 1 h. The primary anti-BAX antibody (1:1000) and anti-VEGF antibody (1:100) (Dallas, TX, USA) were then added for 24 h, followed by the secondary antibodies (1:5000) for 2 h. After establishing the reaction with DAB for 2–3 min, sections were stained with hematoxylin for 2–5 min.

Western blot analysis

Incubation of liver tissues in RIPA Lysis buffer, where whole-cell lysates were prepared (1% NonidetP40, 1% Triton X-100, 0.5% Na deoxycholate, 150 mM NaCl, 1 mM PMSF, 5 mM EDTA, 10 mM EGTA, 50 mM Tris HCl, and 1% leupeptin/pepstatin protease inhibitor cocktail), was used to homogenize liver samples. Protein aliquots were separated using SDS-PAGE (10%) before being transferred to a nitrocellulose membrane. After blocking with 5% skim milk in tris buffer saline containing 0.05% Tween 20, the membranes were treated with primary antibodies (monoclonal (1:1000) anti-NRF2, primaries mouse (1:100) VEGF, (Dallas, TX, USA)-for overnight at 4°C. After that, the membranes were incubated for 1h at 24°C with goat anti-mouse IgG-HRP -and conjugated secondary antibodies (Dallas, TX, USA) in the blocking solution (Atia & Alghriany, 2021).

Bone marrow aspirate procedure

A random sample of BM aspirates (BMAs) was isolated from the femur smears and immediately prepared by washing in serum for differential cell counting within 2–3 min of the animal's death. Marrow assessment was conducted by preparing three to five hematoxylin and eosin (H&E)-stained smears per animal after being fixed in 70% alcohol. Differential BM was magnified and randomly imaged at high microscopic power (40×, oil objectives 100×), Then manually counted (Elmore, 2006).

Statistical analysis

Data were checked for normality (using Anderson–Darling test) and analyzed via one-way analysis of variance, followed by multiple comparisons (Student t-test) in Graph Pad Prism (version 8.4.3 (686); Graph Pad Software, Inc., USA). Software Fiji/Image J for graph image and data from at least three separated experiments were reported as mean ± standard error (SE). Statistical analyses were performed using Prism software (version 8.0.1; GraphPad Software, Inc San Diego, CA, USA).

RESULTS
AD-MSC characterization

On day zero of culture, AD-MSCs were seen to be circular and suspended (Figure 1a). Three days after differentiation, the cells formed thin attached spindles (Figures 1b and c). Several AD-MSCs appeared spindly during passage 1 (P1) (Figures 1d and e); the other cells formed small colonies in passage 2 (P2) (Figures 1f and g), and in passage three (P3), fibroblastic cells (Figures 1h and i). The immunocytochemistry results of AD-MSCs at P3 for CD105 (Figures 2a and b) and CD90 (Figures 2c and d) show a brown dot (positive) localization to AD-MSC nuclei and cytoplasm, in contrast to CD45 (negative) (Figures 2e and f).

Changes in HCC morphology, microscopy, and body weight

In the control group, rat morphology, gross liver assessment, and body weight (BW) appeared normal (Figures 3a–c). Rats induced with HCC displayed morphological and physical changes that appeared to be various degrees of desire for feeding, loss of hair, dormancy, slouched pose, ventro-lateral prostration, hardening in breathing, and emaciation, as shown in Figure 3d. Gross assessment of the liver shows massive changes and an enlarged hepatic surface with rounded borders, darkened liver parenchyma, and soft yellow-brown multinodules, as illustrated in Figures 3e and f. HCC showed a significant decrease (19.77%) in the body weight ratio compared G1, as shown in Figure 3c.
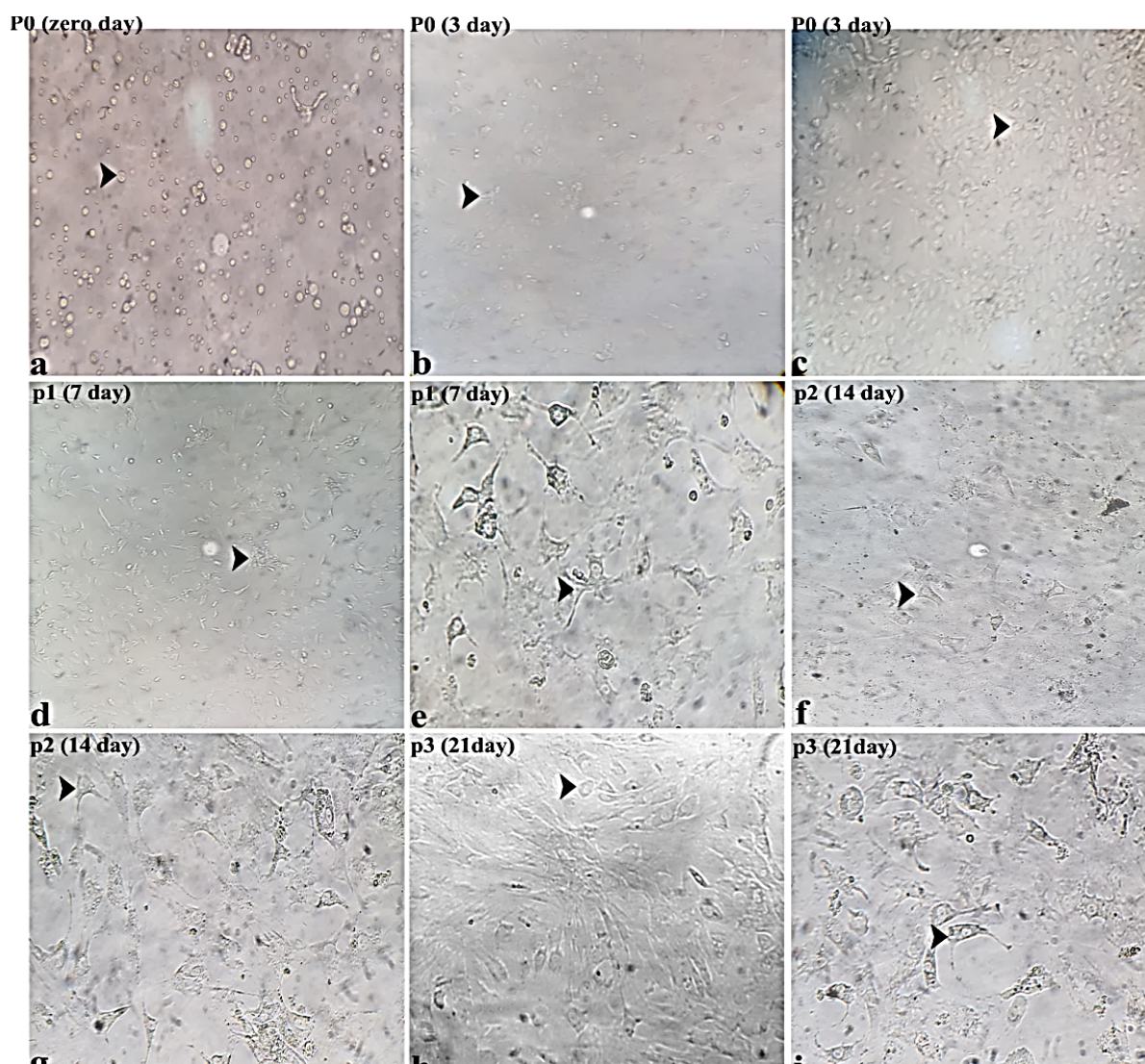
Figure 1. (a to i) Identification of AD-MSCs using phase-contrast microscopy on various days and passages. AD-MSCs were identified by their expansion and morphology. The arrows reveal the AD-MSC (200× and 400×).

Interestingly, AD-MSC transplantation revealed a remarkable enhancement, restoring morphological features and physical behavior (Figure 3g), and the gross morphology with fewer or no nodules (Figures 3h and i). The rat weight ratio was significant decrease and non-significant increased (13.03% and 10.27%) in the therapeutic group compared with G1 and G2, respectively (Figure 3c).

Histopathological lesion

Staining of liver sections by H&E in the control group revealed the normal structure of the liver (Figure 4). Cords of polygonal hepatocytes appeared radiating from the central vein (Figure 4a). These cords are separated by blood sinusoids with endothelial lining (Figure 4b). The portal area contained the portal vein, hepatic artery, and branches of the bile duct (Figure 4c). In the HCC group, there was obvious disorganization of hepatic lobules (Figures 5a and 5b) with the appearance of many blood vessels that were surrounded by cellular proliferation. The parenchyma of the liver is composed of masses of cells of variable shapes and sizes (Figure 5b). Some hepatocytes were large, vacuolated, and irregular. Other cells showed fatty deposition. The nuclei of the cells showed variable changes (margination and fragmentation). Cells with dark rounded nuclei and clear cytoplasm were observed (Figure 5c). Notably, rats with HCC had disrupted lobular architecture and statistically high significantly scoring values ($P < 0.001$) of histopathological change (18.48% ± 2.07% for HCC 0.5% ± 0.3% for Control) (Figure 6d).
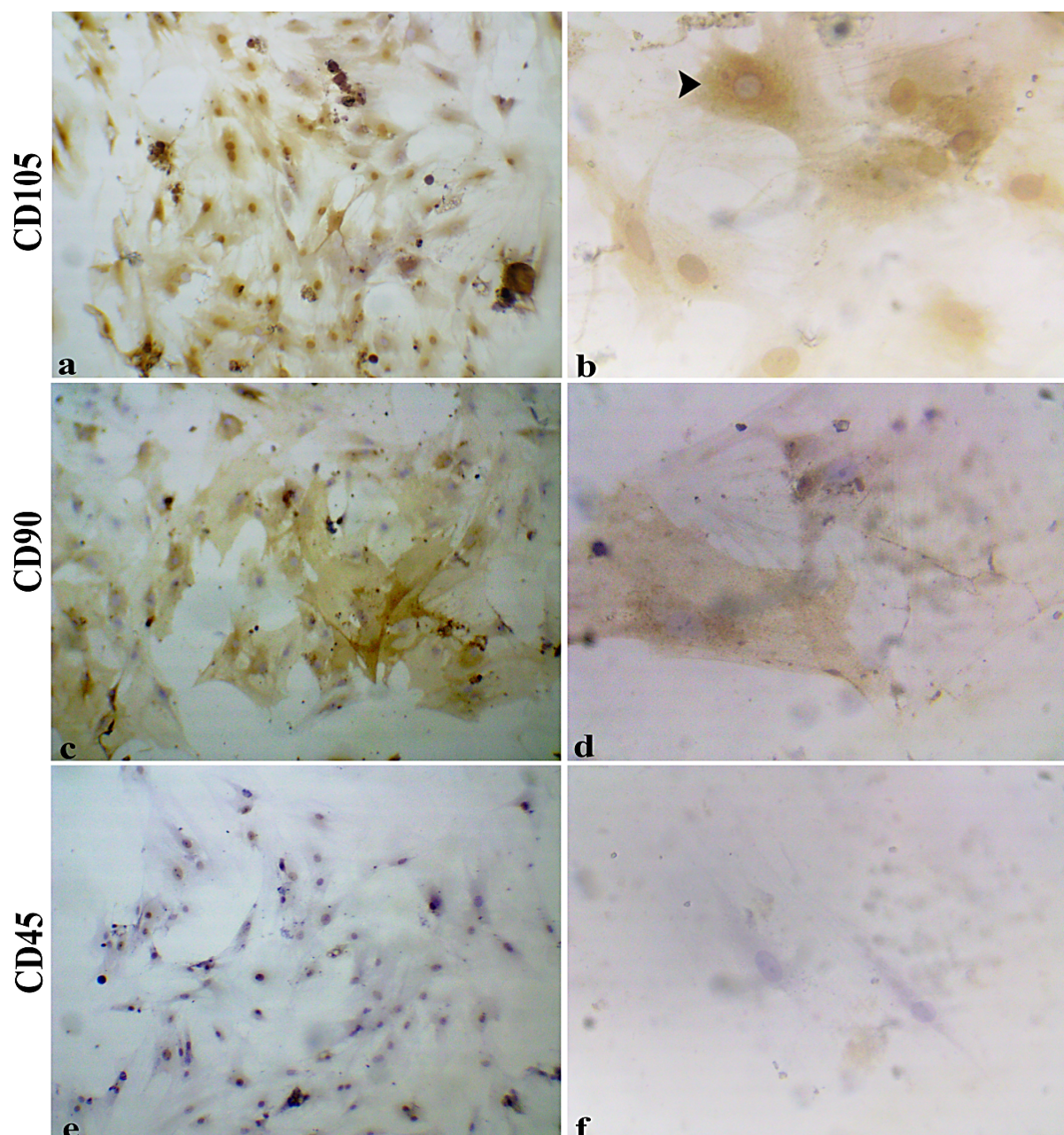
Figure 2. AD-MSCs immunocytochemical staining showing; (a and b) positive CD105 and (c and d) CD90 expression and (e and f) negative CD45 expression (200× and 400×).

In the AD-MSC group, the liver architecture appeared nearly normal (Figure 6a). The cords of hepatocytes were radiated from the central vein. The cords were separated by blood sinusoids. Few hepatocytes with irregular nuclei were observed (Figure 6b). The portal area includes the portal vein, hepatic artery, and branches of the bile duct (Figure 6c). A few cells with dense irregular nuclei were observed (Figures 6b and c). By contrast, AD-MSCs successfully enhanced and restored the hepatic cords with statistically low scoring values of

histopathologic changes (10.60% ± 4.12) compared with the HCC group (P < 0.001) (Figure 6d).

The score for liver fibrosis

Staining of liver sections by Masson's trichrome stain in the control group showed a normal distribution of collagen fibers represented by green color around the central vein and blood sinusoids (Figures 7a and b). In the HCC group, there was a dense increase in the collagen fibers (98.13%) all over the tissue, which lost their normal architecture (Figures 7c, d, and g).
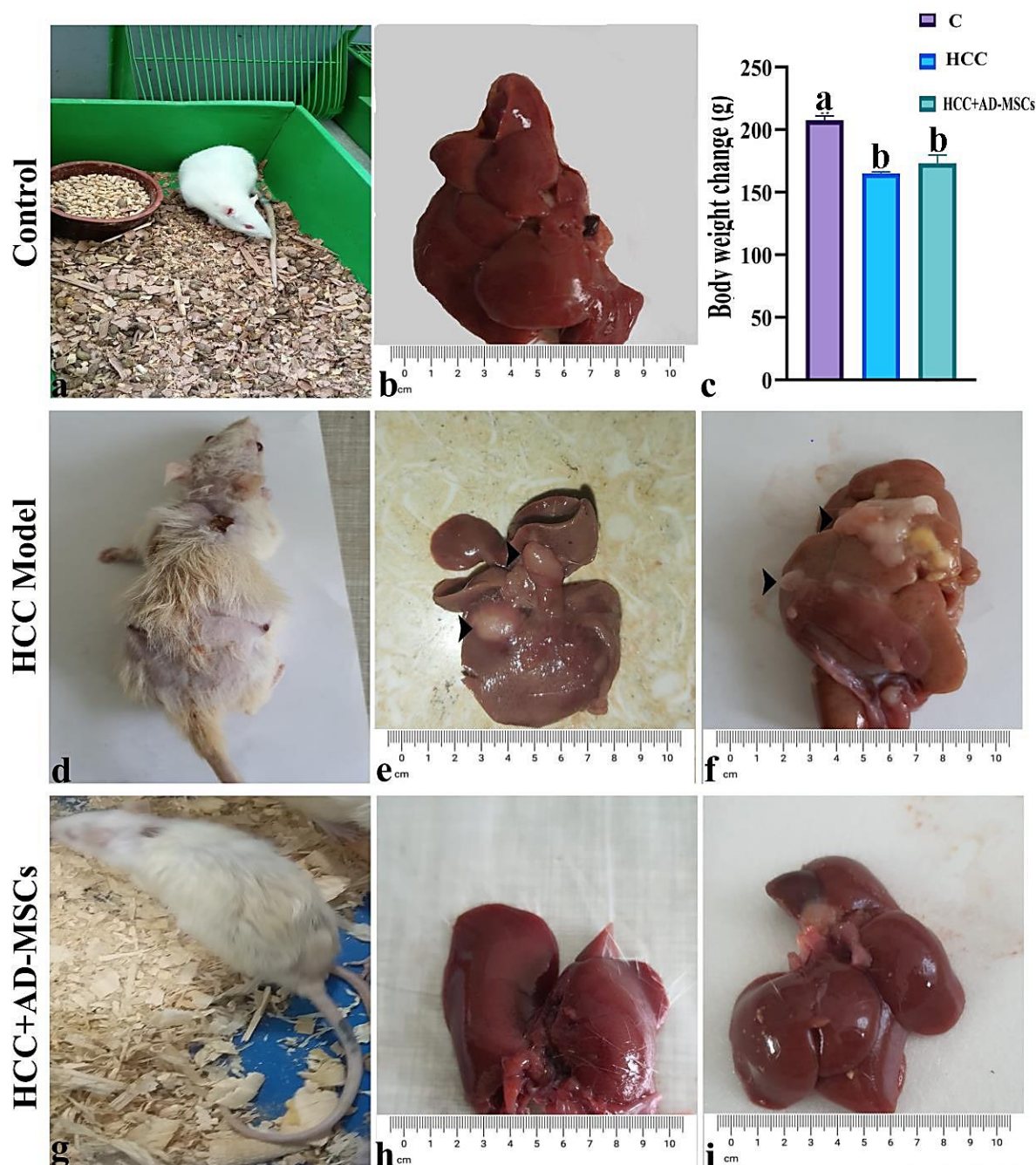
Figure 3. Pathomorphological symptoms in female rats: (a and b) control groups appeared to have normal morphology and liver macroscopically. (c) The experimental groups' average significant change in body weight (p < 0.001). (d) Hair loss, ventro-lateral prostration, emaciation, and dull eyes in the HCC model group; (e and f) enlarged HCC hepatic surface with soft yellow-brown multimodule (arrow); and (g to i) normal morphological features in the MSC group.

In the AD-MSC group, a nearly normal amount of collagen fibers (38.03%) like a control group around the central vein and blood sinusoids was observed (Figures 7 e, f, and g).

Biochemical and tumor marker assay

Among the quantitative data of serum ALT, AST liver function, and AFP tumor marker, there was a significant (P<0.001) elevation in ALT, AST, and AFP levels arranged sequentially (89.92%, 276.28%, and 200.08% vs. G1) when the model group of HCC that received DEN and CCL$_4$ stimulated carcinogenesis. Nonetheless, AD-MSC transplantation resulted in a significant (P<0.001) reduction and restoration of ALT, AST, and AFP levels to nearly normal levels (4.73%, 49.73%, and 46.55% vs. G1; 50.72%, 46.68%, and 37.5% vs. G2) (Figure 8).
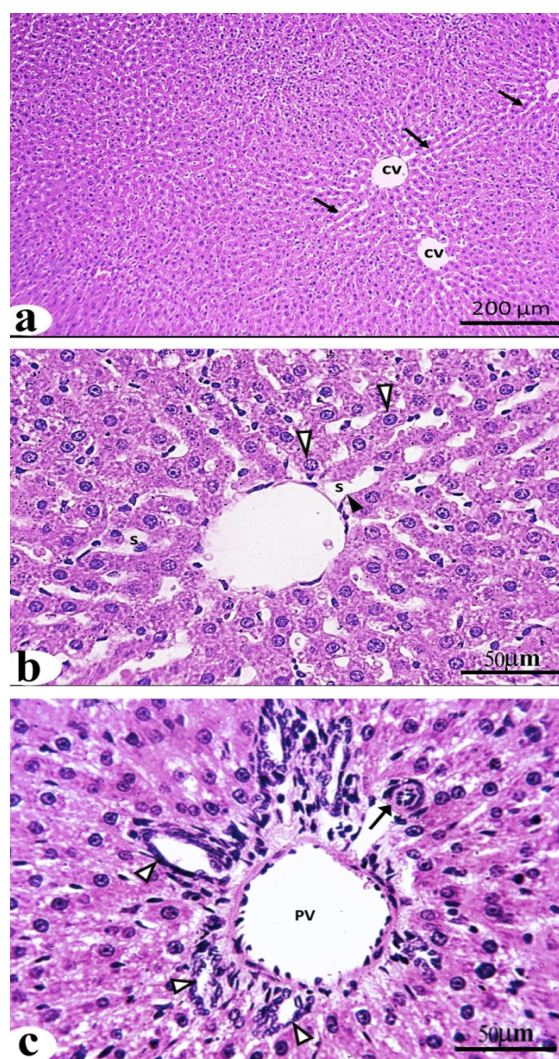
Figure 4. Photomicrographs in liver sections of the control group. b: central vein (CV) from which radiate cords of hepatocytes (↑); b: polygonal hepatocytes (Δ) separated by blood sinusoids (s) with endothelial lining (▲); C: the portal area contains portal vein (PV), hepatic artery (↑), and branches of the bile duct (Δ) (bars, 200 and 50 μm, respectively).

Immunohistochemistry of VEGF and BAX

The immunoreactivity of VEGF and BAX was detected in DAP staining remarkably; normal reactions in the control group (Figures 9 and 10a). The HCC model group treated with DEN and CCl_4 significantly (P<0.001) up-regulated (79.44% vs. G1) levels of VEGF appeared as sinus invasion and severe positive reactions in different patterns of tumor liver cells (Figures 9b and c). By contrast, proapoptotic BAX was abnormally downregulated (38.53% vs. G1), and the expression protein level rate had a negative reaction in the tumor cell's cytoplasm (Figures 10b, c).
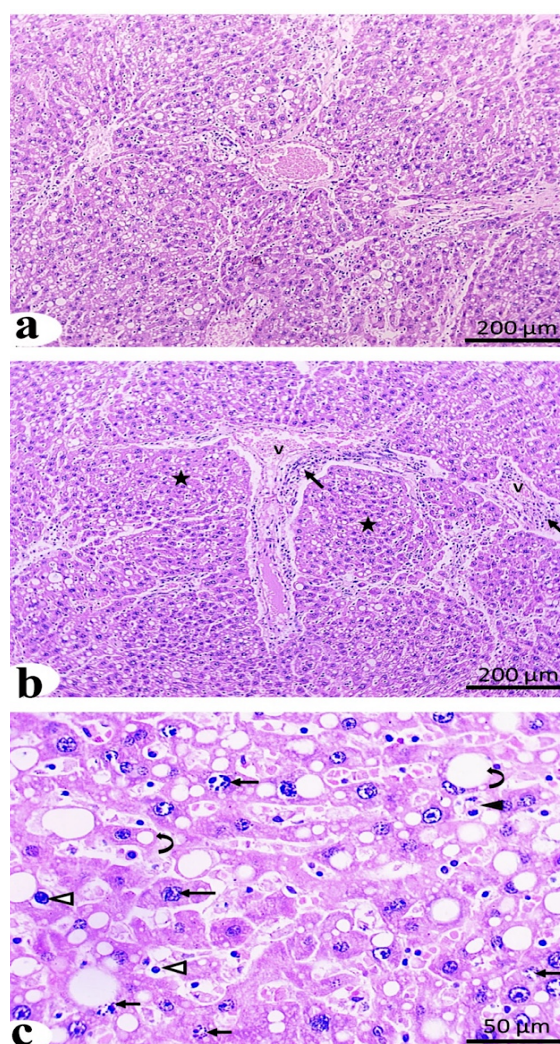

Figure 5. Photomicrographs in liver sections of the HCC group. a: disorganization of hepatic lobules; b: extensive vasculature (v) surrounded by numerous cellular proliferation (↑), and masses of various cells (asterisk); c: hepatocytes exhibit numerous nuclear changes (↑), cytoplasmic fatty deposition (curved arrow), a mitotic figure (▲), and numerous.

Interestingly, AD-MSC transplantation in the HCC group revealed a significant (P<0.001) downregulation of VEGF levels (19.32% and 53.3%) (Figures 9d-f), whereas BAX was upregulated (26.21% and 120.5%) vs. G1 and G2, respectively (Figures 10d-f).

Immunoblot expression of VEGF and Nrf2

By using antibodies that specifically target VEGF and Nrf2, we examined the influence of AD-MSCs on these signaling pathways throughout HCC. Remarkably, the model group of HCC treated with DEN and CCL_4 exhibited a significant (P<0.001) overexpression of VEGF level and Nrf2 of 47.41% and 42% vs. G1,
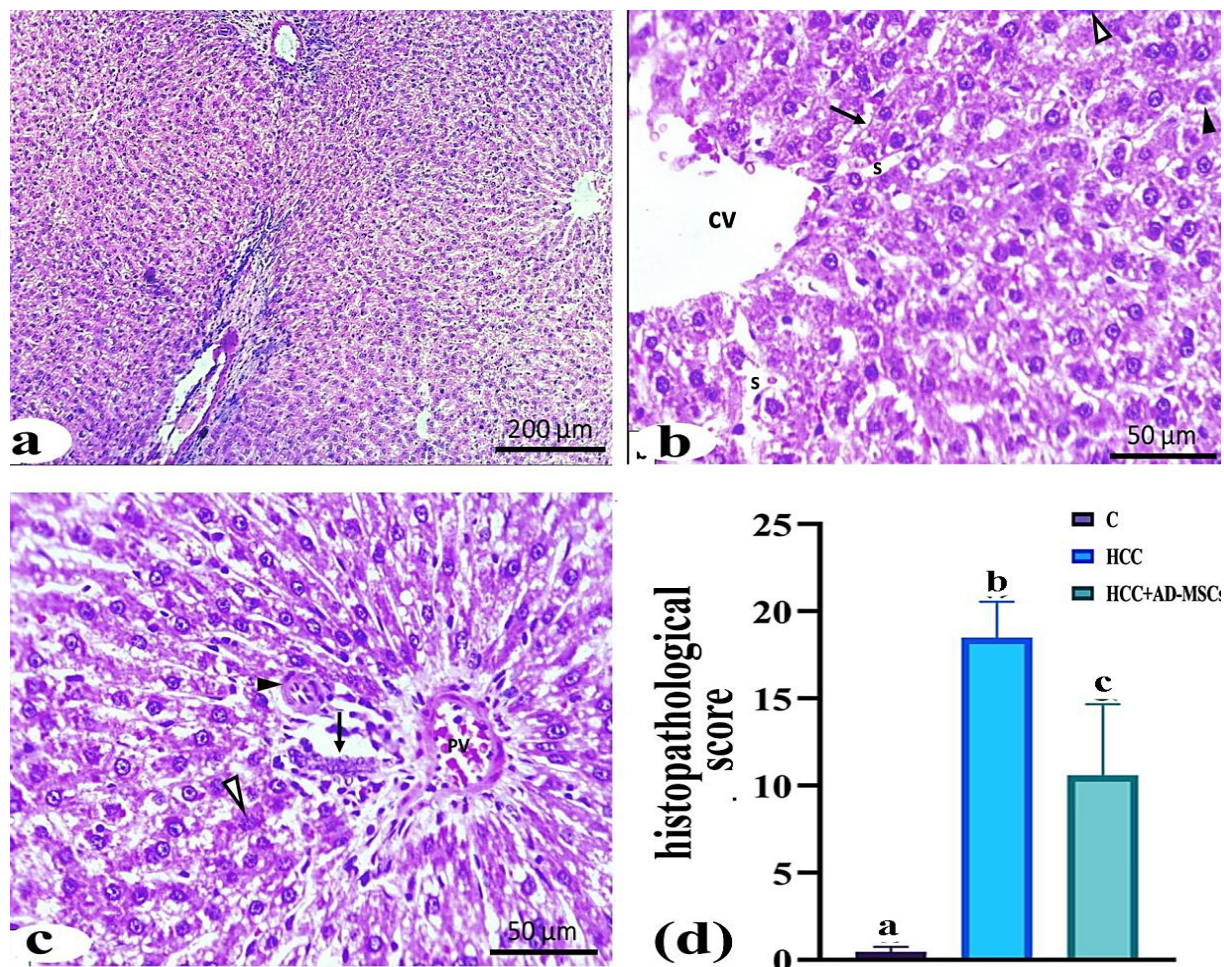
Figure 6. Photomicrographs in liver sections of the AD-MSCs group. a: nearly the appearance of the normal architecture of the liver; b: cords of hepatocytes (↑) radiate from the central vein (CV), blood sinusoids (S), and a few cells with irregular nuclei (Δ); c: the portal area contains portal vein (PV), the hepatic artery (▲), bile duct branches (↑), and a few cells with dense irregular nuclei (Δ) (bars, 200 and 50 μm, respectively); d: the experimental groups' liver histopathology scores; Bars with different signs are significant (P < 0.001).

respectively, based on densitometric measurement. By contrast, the therapeutic group showed a significant (P < 0.001) decrease in the levels of VEGF and Nrf2 (18.55%, and 42.4%) compared with G2, respectively (Figure 11). But the levels of VEGF and Nrf2 significantly increased 16.71% and decreased 18.2% respectively compared with G1 (Figure 11). The protein levels of the immunoblots of VEGF and NRF2 had become normalized to total levels of β-Actin protein.

Determine whether a certain level of citric acid can contribute to an accelerated hepatocyte death, DNA laddering assay was performed to identify apoptosis. The result shown in Fig. 3 revealed that DNA laddering, which is indicative of apoptotic events, occurred in hepatic cell samples from three treated groups, whereas cell apoptosis in the control sample was not detected. In detail, DNA laddering was much more apparent in high dosage group (Lane H) than in the other two dosage groups. Analysis of the results indicated that the apoptotic effect of citric acid on hepatocytes was dose-dependent determine whether a certain level of citric acid can contribute to an accelerated hepatocyte death, DNA laddering assay was performed to identify apoptosis. The result shown in Figure 3 revealed that DNA laddering, which is indicative of apoptotic events, occurred in hepatic cell samples from three treated groups, whereas cell apoptosis in the control sample was not detected. In detail, DNA laddering was much more apparent in high dosage group (Lane H) than in the other two dosage groups. Analysis of the results indicated that the apoptotic effect of citric acid on hepatocytes was dose-dependent

Cytological evaluation of nucleated Bone marrow cells

The total BM and developmental series, which included lineages of neutrophil- granulocytes (myeloblasts and promyelocytes), erythrocytes maturation process (proerythroblast, basophil - erythroblast, poly-erythroblast, and ortho-erythroblast), MKs, megakaryocytes, and other cell counts, showed hypocellularity in the HCC model group. However, neutrophilic (myelocyte, metamyelocyte, band, and seg) appeared to have hypercellularity. Nevertheless, the AD-MSC therapeutic group revealed a marked improvement in the mean of BM composition of the total and differential cell counts with significant value (P < 0.001). They increased compared with the G2 group. However, no significant decrease was observed when compared with G1. Whereas neutrophil (myelocyte, metamyelocyte, Band, Seg, and immature erythrocytes) decreased significantly (P < 0.001) in the therapeutic group compared with the G1 and G2 groups (Table 1).

BM maturation index ratio

According to the present findings, the proportion of the maturity index ratio for hematopoietic cell lineage was counted in the total population and decreased by 0.166 in I: Mg and by 1.828 in I: Me. However, MMI (1/I: Mg) and EMI (1/I: Me) showed an abnormal increase with values of 6.029 and 0.547, respectively, in the HCC model group compared with the G1 control group. Conversely, in the AD-MSC therapeutic group, the maturity index ratio was restored noticeably with a slight increase of 0.188 in I: Mg and a decrease (1.456) in I: Me, whereas MMI (1/I: Mg) and EMI (1/I: Me) showed a decrease (5.333) and (0.687) vs. G1 and G2 groups, respectively (Table 2).

DISCUSSION

The present investigation discovered that AD-MSCs can protect the liver from the harmful effects of DENA/CCL$_4$-induced HCC. These findings are consistent with previous studies which reported that MSCs have antioxidant, immunomodulatory, and anti-inflammatory properties (Mawrie et al. 2019). AD-MSCs have been shown to lower apoptotic protein levels (Atia & Alghriany 2021; Angeloni, et al., 2020). Also, qualitative assays were used to determine the characterization of AD-MSCs in vitro exposure to specific culture conditions. A variety of isolation and characterization approaches have arisen, and flow cytometry was used to identify the antigen expression in hMSCs, which included CD45, CD90, and CD105 (Baghaei et al. 2017).

Table 1. The total BM and developmental series of female rat in different groups of the experiment.

Item	C Mean± SE	HCC		HCC+ AD-MSCs		
		Mean± SE	% of change vs. Control	Mean± SE	% of change Vs. Control	% of change Vs. HCC
TBM	4101±292 a	1698±156 b	58.6% ↓	2668±66.6	34,9% ↓a	57.1% ↑a
Myeloblast	0.9867±0.1a	0.3156±0.03b	68% ↓	0.5422±0.04	45% ↓a	71.8% ↑b
Promyelocyte	1.449±0.2 a	0.6489±0.03b	55.2% ↓	1.022±0.1	29.5% ↓c	57.5% ↑a
Neut- Myelocyte	1.467±0.3 a	3.373±0.2 b	129.9% ↑	1.613±0.2	10% ↑a	52.2% ↓a
Neut-Metamyelocyte	2.733±0.1a	3.467±0.2 a	26.9% ↑	2.576±0.2	5.7% ↓a	25.7% ↓a
Band Neutrophil	8.320±0.2 a	12.95±0.2 b	55.6% ↑	7.782±0.4	6.5% ↓c	39.9% ↓c
Seg-Neutrophil	5.267±0.7 a	9.733±0.4 b	84.8% ↑	6.587±0.2	25.1% ↑a	32.3% ↑a
Proerythroblast	1.147±0.1a	0.5733±0.02b	50% ↓	0.8933±0.04	22.1% ↓a	55.8%↑c
Baso- Erythroblast	5.542±0.4a	1.507±0.3b	72.8% ↓	2.556±0.1	53.9% ↓c	69.6% ↑c
Poly- Erythroblast	0.8356±0.1a	0.3422±0.1b	59% ↓	0.6044±0.04	27.7% ↓a	76.6% ↑a
Ortho- Erythroblast	2.196±0.3a	0.7956±0.1b	63.8% ↓	1.764±0.1	19.7% ↓a	121.7% ↑b
Megakaryocytic cells	8.667±0.9a	2±0.6b	76.9% ↓	5±0.6	42.3% ↓c	150% ↑c
Other cells	2946±308.6a	968±188.5b	67.1% ↓	1840±53	37.5% ↓c	90.1% ↑c

Data are represented as mean ± SE. Changes in the mean values of protein levels with different letters were significantly different (P < 0.001).

Table 2. Experimental finding of BM maturation index (BMI) for female rats

Group	I:Mg	MMI (1/I:Mg)	I:Me	EMI (1/I:Me)
Control	0.239	4.182	2.206	0.453
HCC Model	0.166	6.029	1.828	0.547
HCC+AD-MSCs	0.188	5.333	1.456	0.687

Estimations of the maturity index ratio; I: Mg, MMI (1/I: Mg), I: Me and EMI (1/I: Me); indicates I, immature; M, mature; I: Mg, immature: mature (granulopoiesis); MMI, myeloid maturation index; I:Me, immature: mature (erythropoiesis); EMI, erythroid maturation index. The values are means of at least three separate experiments.

The previous studies are in agreement with our findings on CD90 and CD105 the characterization of adipose MSCs (Baghaei et al. 2017).

The present study used a combination of a profibrogenic agent, CCL_4, and genotoxic DEN to induce HCC in rats, which mimicked the pathophysiological aspects of HCC in humans (Shou et al. 2015). Furthermore, it has developed a mouse model (DEN/CCL_4) with a high tumor HCC incidence and low death rate that may be used in a short time (8 weeks). For the long duration of 44 weeks of the DEN-induced HCC model, a huge number of cancer nodules on the surface of the liver and ROS generation were observed (Cheng et al., 2020).

Our findings showed severe pathological changes in the morphology of the HCC rat model, which caused various degrees of non-desire for feeding and loss of hair. Furthermore, weight loss could be an indirect marker of declining liver function. These findings are in line with previous findings of Kuchařová et al., (2018) and Aly et al. (2019). In addition, the liver HCC model showed massive changes and an enlarged hepatic surface with rounded borders. According to histopathological findings, DENA/CCL4 caused a damaged architecture of the liver, and lymphocytic infiltration, steatosis, and severe fibrosis are observed. Calderaro et al. (2019) found similar pathological alterations in the liver. This could be attributed to DEN's hepatotoxic impact, which is accelerated by lipid overload in hepatocytes, which increases the development of progressive inflammation, oxidative stress, ROS, and fibrosis (Mokh et al., 2019). Furthermore, ROS encourages activated HSCs and Kupffer cells to produce proinflammatory and profibrogenic factors (Affo et al., 2017; Roehlen et al., 2020).

Interestingly, AD-MSC transplantation modulates liver architecture-induced HCC by DEN and CCl_4, a remarkable enhancement that restores morphological features and physical behavior, and the rat weight ratio was increased in the therapeutic group. Hepatic histopathological alterations and fibrotic changes related to H&E, and Masson's trichrome decreased staining were detected, respectively. Previous studies in mice found similar results; BM-MSC transplantation via the tail or portal veins improves liver cirrhosis (Shi et al., 2017; Farahzadi et al., 2018). Some recent research demonstrated that MSCs release a variety of compounds, including cytokines, growth factors (Liau et al., 2018), nitric oxide, and prostaglandin E2 (Fathi et al. 2016), that boost antioxidant defenses, limit oxidation factors (Pulavendran et al. 2010) and anti-inflammatory actions (Fathi et al. 2019).

Based on our findings, DEN/CCl_4-induced oxidative stress can cause liver tissue damage and so alter its enzymatic function; elevating activities of ALT, AST, and AFP in the serum of HCC rats, which can lead to the impairment of liver function. These results were consistent with earlier studies that found a similar rate of HCC in rats given the same DEN/CCl_4 together or DEN-(alone) treated regimen (Mohammed et al., 2014; Hemieda et al., 2016). The increase in AFP levels in HCC-induced rats might be due to hepatic necrosis and subsequent leakage of these enzymes into the circulation from neoplastic cells or irreversibly damaged hepatic cells (Ding et al., 2021). The grading and staging of fibrosis data bolstered our assessment of AD-MSC impacts on liver function indicators, AFP, ALT, and AST levels. According to these findings, AD-MSC transplantation helps the treatment of living fibrosis, which is consistent with earlier research by Truong et al. (2016).
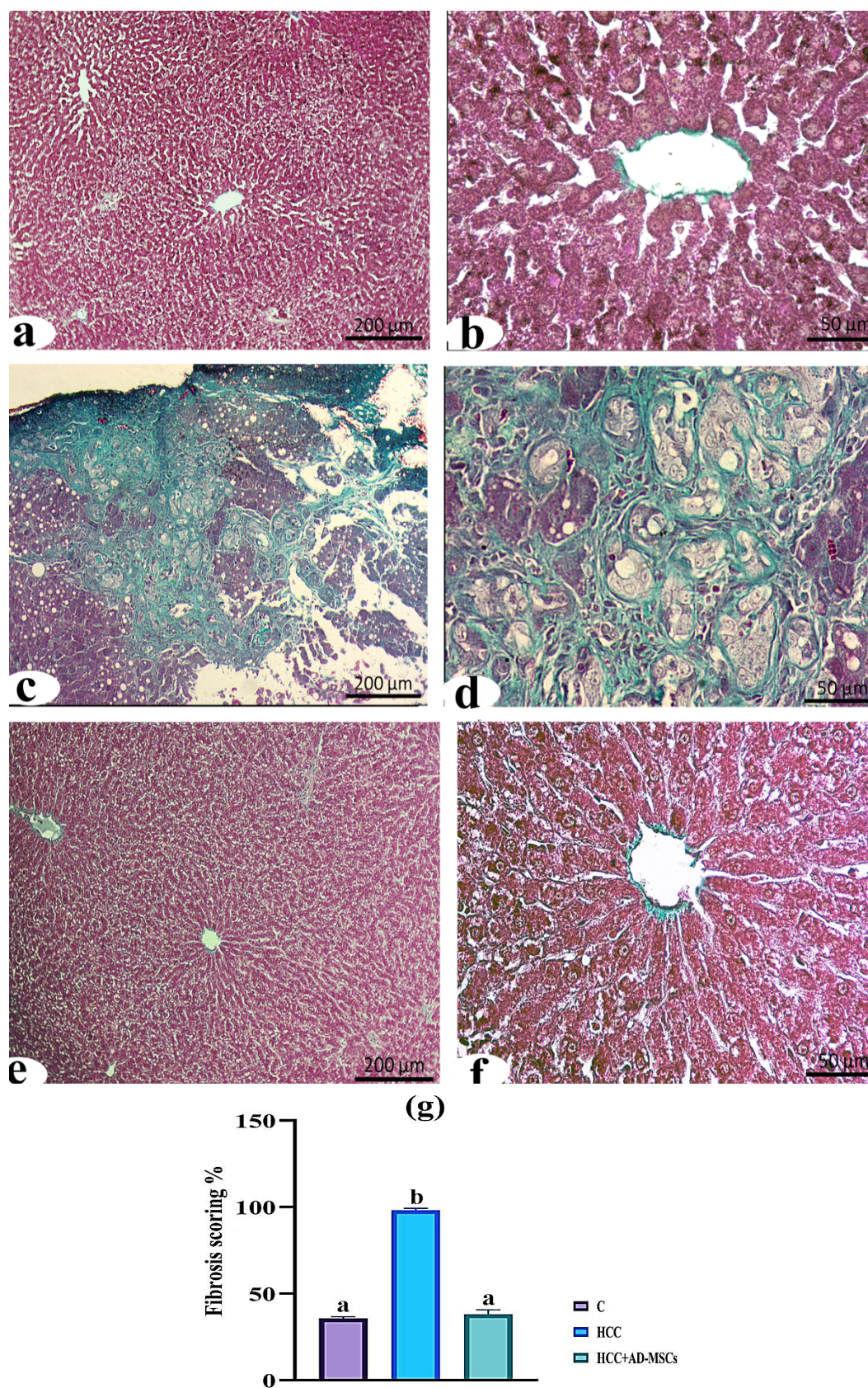
Figure 7. Photomicrographs of liver sections stained by Masson's trichrome stain. a, b: normal collagen fibers around the central vein in the control group; c, d: increased collagen fibers all over the sections in the HCC group; e, f: AD-MSC group showing the nearly normal number of collagen fibers (bars, 200 and 50 μm, respectively); g: histomorphometry scores of liver fibrosis percentage in the experimental groups were displayed as mean ± standard error. Bars with different signs are significantly different (P < 0.001).
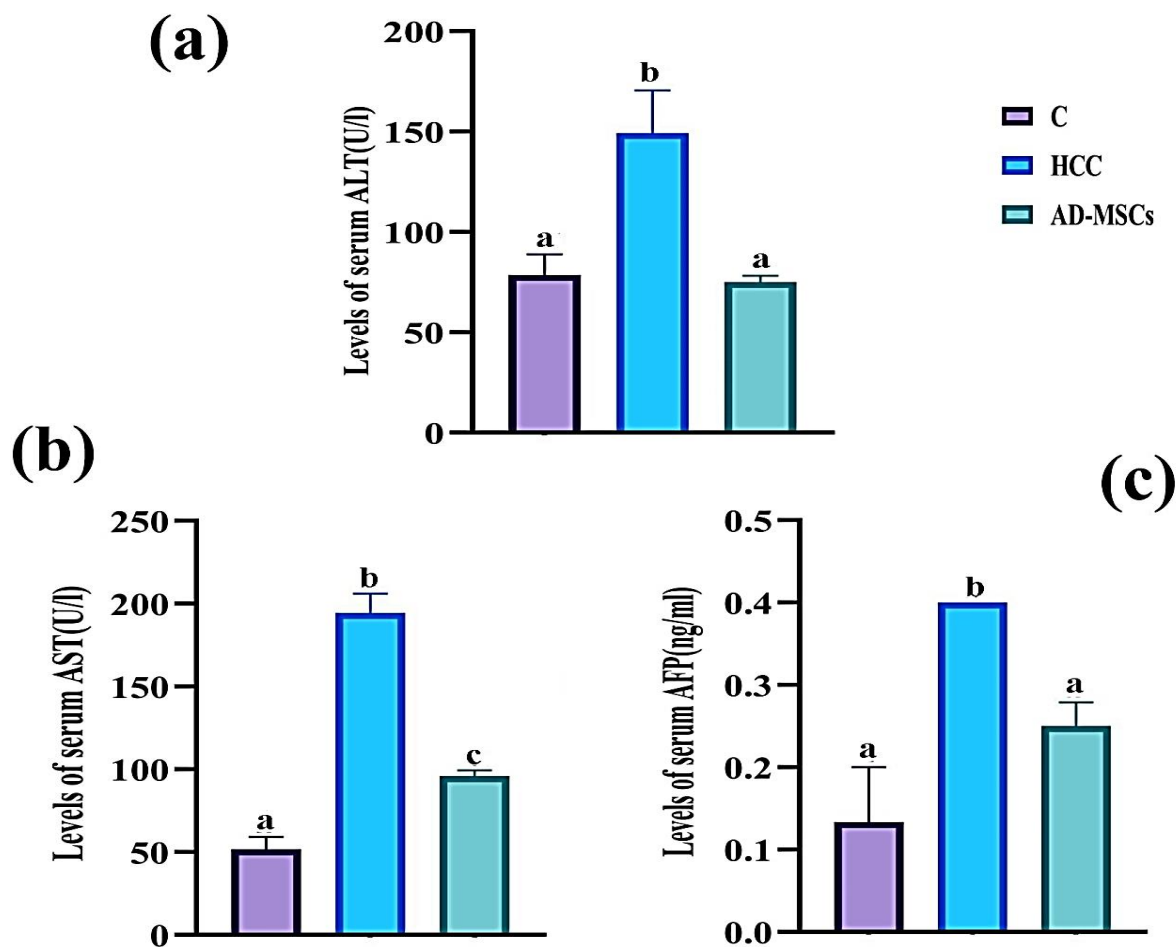
Figure 8. (a) The serum ALT, (b) AST, and (c) AFP tumor markers in the groups were significantly different (p < 0.001). The data were presented the mean ± standard error.

Treated CCl₄ animals' model with ADMSCs had lower levels of ALT, AST, and IL-6 as well as improved histology, and survival rates (Hu et al. 2019).

A dramatic increase in serum VEGF levels, and a decrease in BAX protein levels in the present study may be linked to increased gene transcription and translational processes of apoptotic proteins. This is consistent with Bishayee and Dhir (2009), who reported that the downregulation of BAX immunoexpression was linked to lymph node metastases, and higher tumor stage (Saker et al., 2015; Godlewski et al., 2017). Also, the mechanism of CCl₄ metabolism causes DNA alteration, mitochondrial damage, and even cell death (Xin et al., 2017; Yuan et al., 2018). The high expression of VEGF has been shown to increase HCC by altering the apoptotic pathway (Zhang et al. 2012). Consequently, hypoxia-induced

VEGF upregulation has been recognized as a critical stage in HCC-related angiogenesis (Yakubu et al., 2020) and the production of myeloid inhibitory cells (Wen et al., 2019).

VEGF enhances ROS generation in endothelial cells, which can lead to the activation of Nrf2 by facilitating its dissociation from Keap-1 (Chen et al., 2016) which is consistent with our findings. Also, Li et al. (2016) proposed that VEGF promotes aberrant angiogenesis via the Nrf2/heme oxygenase-1 (HO-1) pathways. According to several studies, the Nrf2 protein upregulates the antiapoptotic protein BCL-₂ and inhibits cellular apoptosis in HepG2 cells (Raghunath et al., 2018) and lung cancer (Solis et al., 2010). Furthermore, elevated Nrf2 expression has been linked to hepatic steatosis and increased lipid deposition in the liver (Zhou et al., 2020), and the development of HCC (Haque et al., 2020).
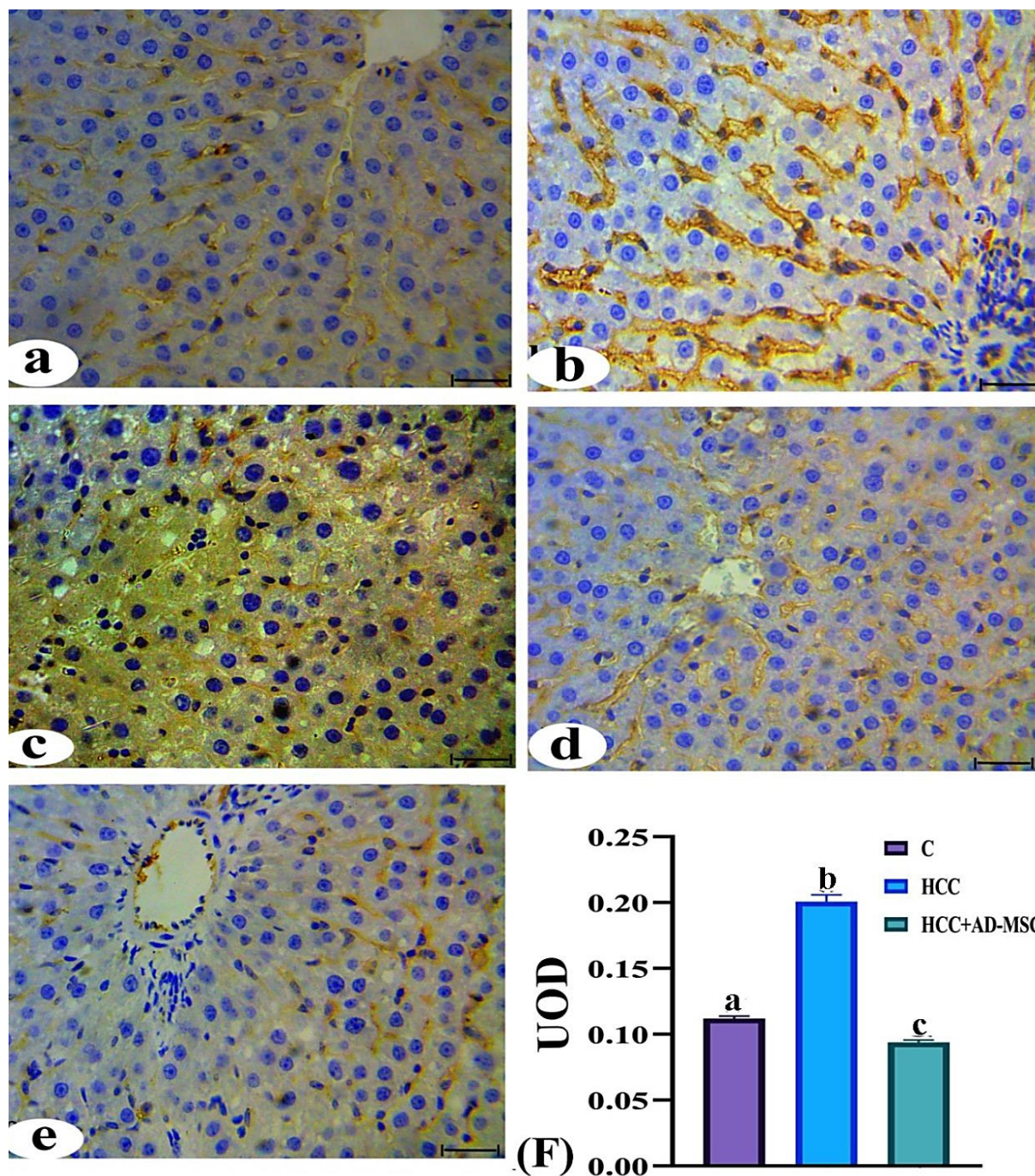
Figure 9. IHC of VEGF protein expression levels in the experimental groups. (a) Control group; (b) HCC model group showed a positive reaction; (c) severe positive reactions indicated tumor cell invasion; (d and e) MSC group showed significant downregulation of VEGF levels nearly as much as the control group. (f) There was a statistically significant difference between the HCC + AD-MSC group and the control or HCC model groups.

The injection of AD-MSCs into HCC rats resulted in the downregulation of both VEGF and Nrf2 expression as well as the upregulation of BAX protein expression in rats. MSCs are one the antiangiogenic medications and play a role in the tumor microenvironment that can be used to restrict tumor development by the expression of chemokine genes (Lee et al.,

2019). Our present *study* provided evidence of BM cells is reduced in the HCC model because of hematopoiesis disruption (Asmaa et al., 2018). Neutrophil activation can lead to angiogenesis and increased blood vessel permeability. Furthermore, immature myeloid cells and neutrophil extracellular traps may promote tumor growth (Strumfa et al., 2018).
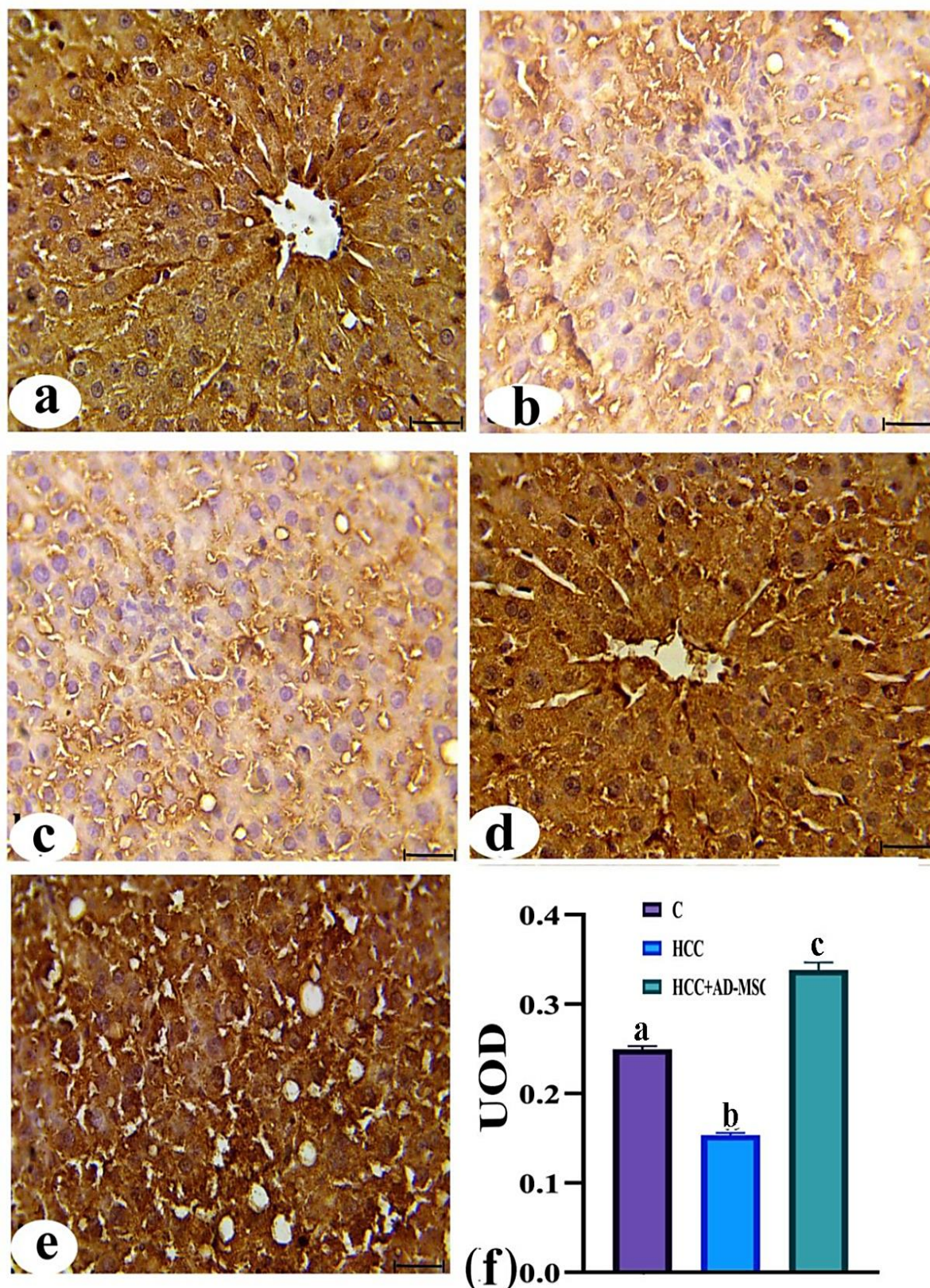
Figure 10. IHC of BAX protein expression levels in the experimental groups. **(a)** The positive reaction distribution in the control group was normal; (b and c) the HCC model group showed a significant negative reaction in the majority of the hepatic cells; (d and e) the MSC group showed remarkable enhancement in the level of BAX protein as huge numbers of brown patches (immunoperoxidase stain, Bar = 50 μm). (f) A statistically significant difference (p < 0.001) was presented by data with different signs.
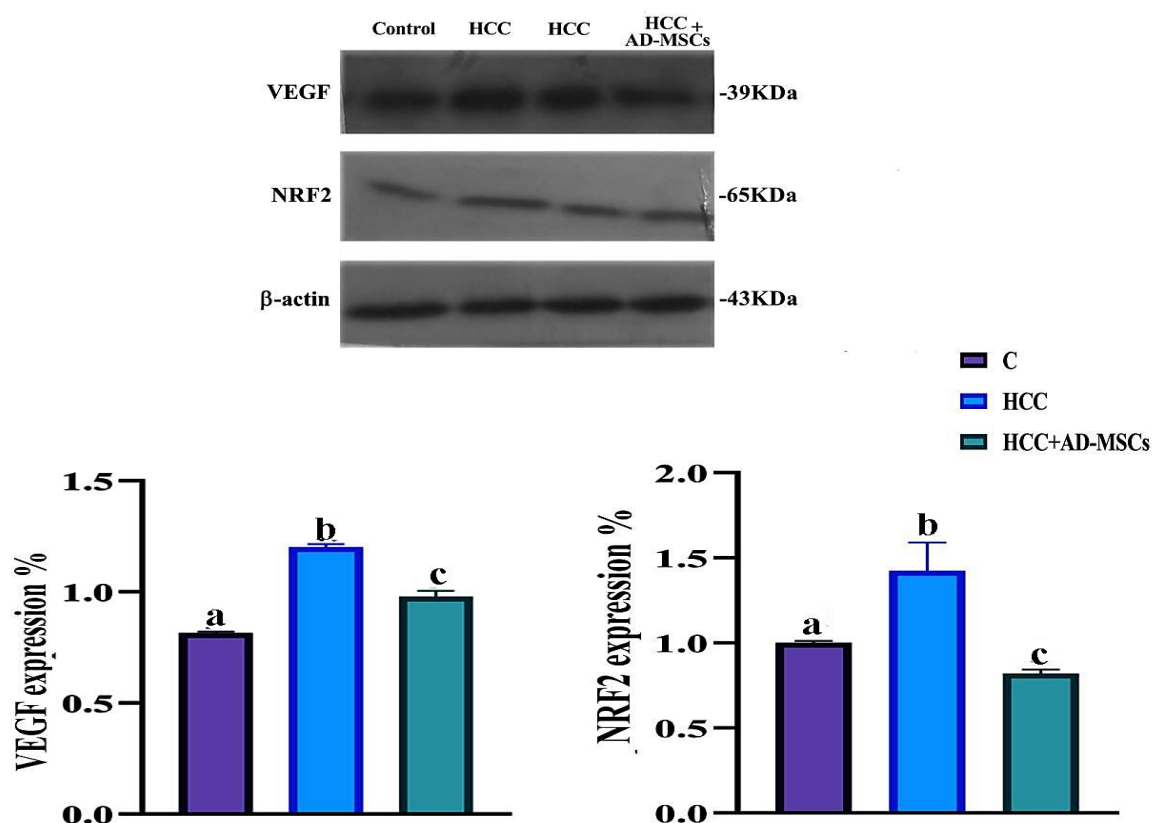
Figure 11. Immunoblot detection shows changes in protein levels of VEGF and Nrf2 in different treatments. Equal protein loading was verified by reprobing stripped membranes with anti-actin. Data with different signs are significantly different (p < 0.001).

The increase in the I: Mg ratio in the HCC groups supported myeloid hyperplasia rather than erythroid hyperplasia in the present investigation, which was most likely attributable to an increase in neutrophilic precursor cells (Trópia de Abreu et al., 2011). Our findings of higher I: M ratio are consistent with the study of Trópia de Abreu et al. (2011) due to a dysfunction of the BM. More critically, in our HCC rat model, we discovered a link between decreased BM cells, increased liver fibrosis, and HCC. The development of liver cirrhosis can impair the BM's hematogenic functions by affecting the erythroid differentiation (Choi et al., 2017). The effect of ADSCs on graft-versus-host disease (GVHD) with better long-term hematopoiesis was demonstrated in a rat model (Jiang et al., 2020). This is consistent with our findings, which showed that after AD-MSC implantation, the maturation index increased hematopoiesis and bone marrow cells. According to the findings of the current investigation, DEN/CCL4 -induced liver cancer might be significantly inhibited by AD-MSC, which also enhances cell recovery.

CONCLUSION

AD-MSC has a substantial inhibitory effect on DEN/CCL4-induced liver cancer and improves cell recovery. The injection of MSCs decreased cirrhosis and increase signs of recovery in the afflicted liver. also, AD-MSC which has a high apoptotic impact on liver cancer blocks the creation of blood vessels and resists immunosuppressive effects in tumors.

ACKNOWLEDGMENTS

DATA AVAILABILITY

All data generated or analyzed during this study are included in this published article.

REFERENCES

Affo, S., Yu, L.-X., & Schwabe, R. F. (2017). The role of cancer-associated fibroblasts and fibrosis in liver cancer. Annual Review of Pathology: Mechanisms of Disease, 12: 153–186.

Aly, S. M., Fetaih, H. A., Hassanin, A. A. I., Abomughaid, M. M., & Ismail, A. A. (2019). Protective effects of garlic and cinnamon oils on hepatocellular carcinoma in albino rats. Analytical Cellular Pathology, 2019.

Angeloni, C., Gatti, M., Prata, C., Hrelia, S., & Maraldi, T. (2020). Role of Mesenchymal Stem Cells in Counteracting Oxidative Stress—Related Neurodegeneration. International Journal of Molecular Sciences, 21(9): 3299.

Arjmand, A., Tsipouras, M. G., Tzallas, A. T., Forlano, R., Manousou, P., & Giannakeas, N. (2020). Quantification of liver fibrosis—A comparative study. Applied Sciences, 10(2): 447.

Asmaa, S. M., Al-Diwan, M. A., & AL-Jadaan, S. A. N. (2018). Hematological profile of rats treated with Quercetin derivative against carbon tetrachloride (CCL4) toxicity. Basrah Journal of Veterinary Research, 17(2): 70-84.

Atia, M. M., & Alghriany, A. A. I. (2021). Adipose-derived mesenchymal stem cells rescue rat hippocampal cells from aluminum oxide nanoparticle-induced apoptosis via regulation of P53, Aβ, SOX2, OCT4, and CYP2E1. Toxicology Reports, 8: 1156–1168.

Baghaei, K., Hashemi, S. M., Tokhanbigli, S., Rad, A. A., Assadzadeh-Aghdaei, H., Sharifian, A., & Zali, M. R. (2017). Isolation, differentiation, and characterization of mesenchymal stem cells from human bone marrow. Gastroenterology and Hepatology from Bed to Bench, 10(3): 208.

Bishayee, A., & Dhir, N. (2009). Resveratrol-mediated chemoprevention of diethylnitrosamine-initiated hepatocarcinogenesis: inhibition of cell proliferation and induction of apoptosis. Chemico-Biological Interactions, 179(2–3): 131–144.

Calderaro, J., Ziol, M., Paradis, V., & Zucman-Rossi, J. (2019). Molecular and histological correlations in liver cancer. Journal of Hepatology, 71(3): 616–630.

Caviglia, J. M., & Schwabe, R. F. (2014). Experimental hepatocarcinogenesis. Pathobiology of Human Disease, 1866–1880.

Chen, J., Yu, Y., Ji, T., Ma, R., Chen, M., Li, G., Li, F., Ding, Q., Kang, Q., & Huang, D. (2016). Clinical implication of Keap1 and phosphorylated Nrf2 expression in hepatocellular carcinoma. Cancer Medicine, 5(10): 2678–2687.

Cheng, C., Shou, Q., Lang, J., Jin, L., Liu, X., Tang, D., Yang, Z., & Fu, H. (2020). Gehua Jiecheng decoction inhibits diethylnitrosamine-induced hepatocellular carcinoma in mice by improving tumor immunosuppression microenvironment. Frontiers in Pharmacology, 11: 809.

Choi, J. W., Ku, Y., Yoo, B. W., Kim, J.-A., Lee, D. S., Chai, Y. J., Kong, H.-J., & Kim, H. C. (2017). White blood cell differential count of maturation stages in bone marrow smear using dual-stage convolutional neural networks. PloS One, 12(12): e0189259.

Ding, H.-F., Zhang, X.-F., Bagante, F., Ratti, F., Marques, H. P., Soubrane, O., Lam, V., Poultsides, G. A., Popescu, I., & Alexandrescu, S. (2021). Prediction of tumor recurrence by α-fetoprotein model after curative resection for hepatocellular carcinoma. European Journal of Surgical Oncology, 47(3): 660–666.

Ding, Y., Liu, K., Xu, Y., Zhao, Q., Lou, S., Xiang, X., Yan, L., Cao, Z., Xie, Q., & Zhu, C. (2020). Combination of inflammatory score/liver function and AFP improves the diagnostic accuracy of HBV-related hepatocellular carcinoma. Cancer Medicine, 9(9:, 3057–3069.

Elmore, S. A. (2006). Enhanced histopathology of the bone marrow. Toxicologic Pathology, 34(5): 666–686.

Farahzadi, R., Fathi, E., Mesbah-Namin, S. A., & Zarghami, N. (2018). Anti-aging protective effect of L-carnitine as clinical agent in regenerative medicine through increasing telomerase activity and change in the hTERT promoter CpG island methylation status of adipose tissue-derived mesenchymal stem cells. Tissue and Cell, 54: 105–113.

Fathi, E., & Farahzadi, R. (2016). Isolation, culturing, characterization and aging of adipose tissue-derived mesenchymal stem cells: a brief overview. Brazilian Archives of Biology and Technology, 59: e16150383

Fathi, E., Sanaat, Z., & Farahzadi, R. (2019). Mesenchymal stem cells in acute myeloid leukemia: a focus on mechanisms involved and therapeutic concepts. Blood Research, 54(3): 165–174.

Galicia-Moreno, M., Silva-Gomez, J. A., Lucano-Landeros, S., Santos, A., Monroy-Ramirez, H. C., & Armendariz-Borunda, J. (2021). Liver cancer: therapeutic challenges and the importance of experimental models. Canadian Journal of Gastroenterology and Hepatology, 2021, Article ID 8837811, 10 pages

Godlewski, J., Krazinski, B. E., Kowalczyk, A. E., Kiewisz, J., Kiezun, J., Kwiatkowski, P., Sliwińska-Jewsiewicka, A., Wierzbicki, P. W., & Kmieć, Z. (2017). Expression and prognostic significance of EP300, TP53 and BAX in clear cell renal cell carcinoma. Anticancer Research, 37(6): 2927–

2937.

Haque, E., Karim, M. R., Salam Teeli, A., Śmiech, M., Leszczynski, P., Winiarczyk, D., et al.,(2020). Molecular mechanisms underlying hepatocellular carcinoma induction by aberrant NRF2 activation-mediated transcription networks: interaction of NRF2-KEAP1 controls the fate of hepatocarcinogenesis. International Journal of Molecular Sciences, 21(15): 5378.

Heijnen, B. H. M., Straatsburg, I. H., Gouma, D. J., & van Gulik, T. M. (2003). Decrease in core liver temperature with 10 C by in situ hypothermic perfusion under total hepatic vascular exclusion reduces liver ischemia and reperfusion injury during partial hepatectomy in pigs. Surgery, 134(5): 806–817.

Hemieda, F., Serag, H. M., El-Baz, E., Ramadan, S., Faried, A. E., Hemieda, S., & Ramadan, M. E. (2016). Therapeutic efficacy of licorice and/or cisplatin against diethylnitrosamine and carbon tetrachloride-induced hepatocellular carcinoma in rats. *Journal* of American *Science,*12: 10–19.

Hu, C., Zhao, L., & Li, L. (2019). Current understanding of adipose-derived mesenchymal stem cell-based therapies in liver diseases. Stem Cell Research & Therapy, 10(1): 1–13.

Ismael, M. N., Forde, J., Milla, E., Khan, W., & Cabrera, R. (2019). Utility of Inflammatory Markers in Predicting Hepatocellular Carcinoma Survival after Liver Transplantation. BioMed Research International, 2019, 7284040. https://doi.org/10.1155/2019/7284040

Javan, M. R., Khosrojerdi, A., & Moazzeni, S. M. (2019). New insights into implementation of mesenchymal stem cells in cancer therapy: prospects for anti-angiogenesis treatment. Frontiers in Oncology, 840.

Jiang, M., Bi, X., Duan, X., Pang, N., Wang, H., Yuan, H., Zhang, R., & Cui, L. (2020). Adipose tissue-derived stem cells modulate immune function in vivo and promote long-term hematopoiesis in vitro using the aGVHD model. Experimental and Therapeutic Medicine, 19(3): 1725–1732.

Kuchařová, V., Daněk, O., Škorič, M., Veselá, I., & Tomenendálová, J. (2018). Organ toxicity of diethylnitrosamine and capsaicin in mice–in vivo study. Annales Universitatis Paedagogicae Cracoviensis Studia Naturae, 3: 39–46.

Lee, M. W., Ryu, S., Kim, D. S., Lee, J. W., Sung, K. W., Koo, H. H., & Yoo, K. H. (2019). Mesenchymal stem cells in suppression or progression of hematologic malignancy: current status and challenges. Leukemia, 33(3): 597–611.

Li, L., Pan, H., Wang, H., Li, X., Bu, X., Wang, Q., Gao, Y., Wen, G., Zhou, Y., & Cong, Z. (2016). Interplay between VEGF and Nrf2 regulates angiogenesis

due to intracranial venous hypertension. Scientific Reports, 6(1): 1–11.

Liau, L. L., Makpol, S., Azurah, A. G. N., & Chua, K. H. (2018). Human adipose-derived mesenchymal stem cells promote recovery of injured HepG2 cell line and show sign of early hepatogenic differentiation. Cytotechnology, 70(4): 1221–1233.

Marchenko, S., & Flanagan, L. (2007). Immunocytochemistry: Human neural stem cells. Journal of Visualized Experiments, 7. https://doi.org/10.3791/267

Mawrie, D., Bhattacharjee, K., Sharma, A., Sharma, R., Bhattacharyya, J., Bhattacharjee, H., Deori, N., Kumar, A., & Jaganathan, B. G. (2019). Human orbital adipose tissue-derived mesenchymal stem cells possess neuroectodermal differentiation and repair ability. Cell and Tissue Research, 378(3): 531–542.

Memon, A., Pyao, Y., Jung, Y., Lee, J. Il, & Lee, W. K. (2020). A modified protocol of diethylnitrosamine administration in mice to model hepatocellular carcinoma. International Journal of Molecular Sciences, 21(15): 5461.

Mohamed, N. Z., Aly, H. F., Moneim El-Mezayen, H. A., & El-Salamony, H. E. (2019). Effect of co-administration of Bee honey and some chemotherapeutic drugs on dissemination of hepatocellular carcinoma in rats. Toxicology Reports, 6: 875–888.

Mohammed, F. Z., Sultan, A. S., & Abas, A. M. (2014). Chemopreventive and therapeutic effect of capsaicin against diethylnitrosamine induced liver injury and hepatocellular carcinoma in rats. Int. J. Biol. Pharm. Res, 5(8): 630–642.

Mokh, A., Abdelhady, D., Ghazy, E., Aboumosalem, H., & Goda, W. (2019). Sesame oil mitigates initiation stage of diethynitrosamine hepatocarcinogenesis in rats. Slovenian Veterinary Research, 56 (Suppl 22): 487–98.

Pernecker, I., Bauer, N. B., Johannes, S., Ginder, M., Harleman, J. H., & Moritz, A. (2017). Comparison of the Sysmex XT-2000iV with microscopic differential counts of canine bone marrow. Journal of Veterinary Diagnostic Investigation, 29(2): 148–153.

Pulavendran, S., Vignesh, J., & Rose, C. (2010). Differential anti-inflammatory and anti-fibrotic activity of transplanted mesenchymal vs. hematopoietic stem cells in carbon tetrachloride-induced liver injury in mice. International Immunopharmacology, 10(4): 513–519.

Qu, W., Wang, Z., Hare, J. M., Bu, G., Mallea, J. M., Pascual, J. M., Caplan, A. I., Kurtzberg, J., Zubair, A. C., & Kubrova, E. (2020). Cell-based therapy to reduce mortality from COVID-19: Systematic review and meta-analysis of human studies on

acute respiratory distress syndrome. Stem Cells Translational Medicine, 9(9): 1007–1022.

Raghunath, A., Sundarraj, K., Arfuso, F., Sethi, G., & Perumal, E. (2018). Dysregulation of Nrf2 in hepatocellular carcinoma: role in cancer progression and chemoresistance. Cancers, 10(12): 481.

Roehlen, N., Crouchet, E., & Baumert, T. F. (2020). Liver fibrosis: mechanistic concepts and therapeutic perspectives. Cells, 9(4): 875.

Saker, Z., Tsintsadze, O., Jiqia, I., Managadze, L., & Chkhotua, A. (2015). Importance of apoptosis markers (MDM2, BCL-2 and Bax) in benign prostatic hyperplasia and prostate cancer. Georgian Medical News, 249: 7–14.

Schwartz, D., Guzman, D. S., Beaufrere, H., Ammersbach, M., Paul-Murphy, J., Tully Jr, T. N., & Christopher, M. M. (2019). Morphologic and quantitative evaluation of bone marrow aspirates from Hispaniolan Amazon parrots (Amazona ventralis). Veterinary Clinical Pathology, 48(4): 645–651.

Shi, D., Lv, L., Fang, D., Wu, W., Hu, C., Xu, L., Chen, Y., Guo, J., Hu, X., & Li, A. (2017). Administration of Lactobacillus salivarius LI01 or Pediococcus pentosaceus LI05 prevents CCl4-induced liver cirrhosis by protecting the intestinal barrier in rats. Scientific Reports, 7(1): 1–13.

Shou, Q., Chen, F., Cai, Y., Zhang, S., Tu, J., Zhang, L., Wang, D., Wang, J., Chen, M., & Fu, H. (2015). Inhibition of diethylnitrosamine-induced hepatocarcinogenesis in mice by a high dietary protein intake. Nutrition and Cancer, 67(7): 1151–1158.

Solis, L. M., Behrens, C., Dong, W., Suraokar, M., Ozburn, N. C., Moran, C. A., Corvalan, A. H., Biswal, S., Swisher, S. G., & Bekele, B. N. (2010). Nrf2 and Keap1 abnormalities in non–small cell lung carcinoma and association with clinicopathologic features. Clinical Cancer Research, 16(14): 3743–3753.

Strumfa, I., Mezale, D., Strumfs, B., Vanags, A., Kalva, A., Balodis, D., Fridrihsone, I., Abolins, A., & Gardovskis, J. (2018). Innovative Blood Tests for Hepatocellular Carcinoma: Liquid Biopsy and Evaluation of Systemic Inflammatory Reaction. In Hepatocellular Carcinoma-Advances in Diagnosis and Treatment. IntechOpen.

Suvarna, K. S., Layton, C., & Bancroft, J. D. (2018). Bancroft's theory and practice of histological techniques E-Book. Elsevier health sciences.

Trópia de Abreu, R., Carvalho, M. das G., Carneiro, C. M., Giunchetti, R. C., Teixeira-Carvalho, A., Martins-Filho, O. A., Coura-Vital, W., Corrêa-Oliveira, R., & Reis, A. B. (2011). Influence of clinical status and parasite load on erythropoiesis and leucopoiesis in dogs naturally infected with Leishmania (Leishmania) chagasi. PloS One, 6(5): e18873.

Truong, N. H., Nguyen, N. H., Le, T. Van, Vu, N. B., Huynh, N., Nguyen, T. Van, Le, H. M., Phan, N. K., & Pham, P. Van. (2016). Comparison of the treatment efficiency of bone marrow-derived mesenchymal stem cell transplantation via tail and portal veins in CCl4-induced mouse liver fibrosis. Stem Cells International, 2016, Article ID 5720413, 13 pages.

Uehara, T., Pogribny, I. P., & Rusyn, I. (2021). The DEN and CCl4-Induced Mouse Model of Fibrosis and Inflammation-Associated Hepatocellular Carcinoma. Current Protocols, 1(8): e211.

Wang, L., Liu, K., Sytwu, H., Yen, M., & Yen, B. L. (2021). Advances in mesenchymal stem cell therapy for immune and inflammatory diseases: Use of cell-free products and human pluripotent stem cell-derived mesenchymal stem cells. Stem Cells Translational Medicine, 10(9): 1288–1303.

Wen, L., Xin, B., Wu, P., Lin, C., Peng, C., Wang, G., Lee, J., Lu, L., & Feng, G. (2019). An efficient combination immunotherapy for primary liver cancer by harmonized activation of innate and adaptive immunity in mice. Hepatology, 69(6): 2518–2532.

Xin, B., Cui, Y., Wang, Y., Wang, L., Yin, J., Zhang, L., Pang, H., Zhang, H., & Wang, R. (2017). Combined use of alcohol in conventional chemical-induced mouse liver cancer model improves the simulation of clinical characteristics of human hepatocellular carcinoma. Oncology Letters, 14(4): 4722–4728.

Yakubu, O. F., Metibemu, D. S., Adelani, I. B., Adesina, G. O., Edokwe, C. B., Oseha, O. E., & Adebayo, A. H. (2020). Annona senegalensis extract demonstrates anticancer properties in N-diethylnitrosamine-induced hepatocellular carcinoma in male Wistar rats. Biomedicine & Pharmacotherapy, 131: 110786.

Yuan, Y., Zhou, C., Chen, X., Tao, C., Cheng, H., & Lu, X. (2018). Suppression of tumor cell proliferation and migration by human umbilical cord mesenchymal stem cells: A possible role for apoptosis and Wnt signaling. Oncology Letters, 15(6): 8536–8544.

Zhang, L., Wang, J.-N., Tang, J.-M., Kong, X., Yang, J.-Y., Zheng, F., Guo, L.-Y., Huang, Y.-Z., Zhang, L., & Tian, L. (2012). VEGF is essential for the growth and migration of human hepatocellular carcinoma cells. Molecular Biology Reports, 39(5): 5085–5093.

Zhou, J., Zhang, X., Tang, H., Yu, J., Zu, X., Xie, Z., Yang, X., Hu, J., Tan, F., & Li, Q. (2020). Nuclear factor erythroid 2 (NF-E2)-related factor 2 (Nrf2) in autophagy-induced hepatocellular carcinoma. Clinica Chimica Acta, 506: 1–8.